Biophysical Chemistry 8 (1978) 317–326

OPTICAL DIFFRACTION STUDY OF MUSCLE FIBERS. II. ELECTRO-OPTICAL PROPERTIES OF MUSCLE FIBERS

Shigeo YOSHINO,
Department of Physics, Faculty of Science, Nagoya University, Nagoya 464, Japan

Yoshiki UMAZUME, Reibun NATORI
Department of Physiology, The Jikei University School of Medicine, Tokyo 105, Japan

Satoru FUJIME and Shuko CHIBA
Mitsubishi-Kasei Institute of Life Sciences, Machida, Tokyo 194, Japan

Received 10 April 1978

When an electric field is applied along the fiber axis, the intensities of all observable optical diffraction lines of skeletal muscle fibers increase. This electro-optical effect was extensively studied and it was confirmed that the effect is due to the interaction between electric dipole moments of thin filaments and the applied field. From the present study on the intensity modulation due to applied field in sinusoidal and square forms, we confirmed that (1) the thin filament is a semi-flexible rod, (2) the second order mode of the bending motion of thin filaments contributes to the electro-optical effect of muscle fibers at higher frequencies of a sinusoidal field or shorter durations of a square field, (3) the induced moment has no appreciable effect, and (4) the estimated value of the flexural rigidity of thin filaments strongly depends on the concentrations of free calcium ions in the myofibrillar space.

1. Introduction

Skeletal muscle fibers act as a diffraction grating to visible light, because regularly spaced repetitive striations in μm order arise from a periodic change in the refractive index along the fiber axis. Optical diffraction studies of muscle fibers have extensively been made by many authors. In this communication, we will give experimental results on an electro-optical effect in muscle fibers.

Each thin filament has a permanent dipole moment directed from the Z-line to the opposite end. When the external electric field is applied along the fiber axis, the thin filament reorients its direction relative to the direction of the applied field [1]. Then the concentration of proteins, or refractive index, of an I-band on one side of the Z-line increases and that on the other side decreases. This change in the refractive index of I-bands causes an intensity increase of diffraction lines as discussed in [1] and in part I of this series [2].

The thin filament or F-actin (a main component of thin filaments) was proposed to be a semiflexible rod [3,4], and the flexural rigidity of thin filaments has been measured *in vitro* [5,6] and *in vivo* [1]. In *in vitro* experiments, however, the existence of aggregation and the exponential length distribution of actin filaments make the analysis very difficult. In *in vivo* experiments, on the other hand, absence of aggregation, the monodispersity of the thin filament length and the regularity of the muscle structure make it simple to treat the system. The flexural rigidity of thin filaments *in vivo* has been estimated from the relaxation time of the electro-optical effect after turning off the applied electric field [1].

If the physical model in [1] is valid, the second order mode of the bending motions will also contribute to the electro-optical effect. We will show the validity of our model discussed in part I [2].

The physical principle included in the present electro-optical effect is very similar in many respects to that of transient electric birefringence or the Kerr -

effect [7]. The essential difference lies in that the effect comes from the interference of scattered light in the former and from optical anisotropy of the solution as a whole in the latter.

2. Experimental

2.1. Principle of experimental techniques

As stated in detail in [2], the principle of our measurements is as follows. The external electric field parallel with the fiber axis reorients the thin filaments and this results in an increase of the intensities of diffraction lines. For a cosine field in time, the response may be written from eq. (58) in [2] as

$$\Delta I(u_n, t) \propto B_\omega \cos(\omega t - \phi_\omega) + B_{2\omega} \cos(2\omega t - 2\phi_{2\omega}). \quad (1)$$

When we use a lock-in detector in its ω-mode, the output of the detector is proportional to $B_\omega \cos(\theta - \phi_\omega)$ where θ is the phase angle of the detector. When we use the detector in its 2ω-mode (or its harmonics mode), the output of the detector is proportional to $B_{2\omega} \cos(\theta - 2\phi_{2\omega})$. In any case, we can determine the phase shift θ which gives the maximum output of the detector. (Actually we read the phase shift θ which gives a zero output of the detector. Then we have, for example, $\phi = \theta - \pi/2$.) In this way, we can obtain the ϕ_ω versus ω or $\phi_{2\omega}$ versus ω relation.

For square field, on the other hand, the analysis of the response encounters a difficulty. Only when $\Delta I_1(u_n, t) \gg \Delta I_2(u_n, t)$ or *vice versa* (see eqs. (47) and (48) in [2]), does the analysis become easier. Actually, the intensity of the first order line of muscle fibers at sarcomere lengths around 8 μm is very low [1], so that the condition $\Delta I_2(u_1, t) \gg \Delta I_1(u_1, t)$ is realized. In such a case, for example, the response may be written from eq. (48) in [2] as

$$\Delta I(u_1, t) \propto \left[\sum_k R_k \exp(-t/\tau_k)\right]^2 \quad (2)$$

In order to see the effect of higher order modes, especially that of the $k = 2$ mode, we can analyze the experimental data by a cumulant expansion technique [8], which gives us the initial decay rate of the response (see eq. (51) in [2]).

2.2. Preparation of muscle fibers

Three kinds of fibers from semitendinosus muscle of frogs (*Rana catesbeiana*) were used; single, skinned and glycerinated fibers.

A single fiber was isolated and placed on a glass slide and was quickly covered with a layer of liquid paraffin oil. The single fiber was stretched up to 6 μm in sarcomere length.

To prepare skinned fibers, Natori's method was applied [9]. After the sarcolemma was removed mechanically with a knife, the skinned fiber was stretched up to 7 μm in sarcomere length. About 0.5 μl saline solution (107 mM methanesulfonic acid potassium salt, 4 mM magnesium sulfate and 20 mM Tris maleate buffer, pH 6.8) was applied to the skinned fiber for 30 min and the solution around the fiber was removed with a piece of filter paper after swelling of the fiber.

Fiber bundles for glycerination were obtained from the same muscle. The bundle was bound to a glass rod in the stretched condition (sarcomere length of 3.5 μm). It was then immersed in 50% glycerol/water with 2 mM EGTA (ethylene glycol bis(β-amino ethyl-ether)-N,N'-tetraacetic acid) and 5 mM phosphate buffer at pH 6.8. After 24 hr at 0°C, it was transferred to fresh glycerol/water and stored at −20°C for at least four weeks before use. A single fiber was dissected from this glycerinated bundle and was washed five times with Ca^{2+}-free solution (107 mM methanesulfonic acid potassium salt, 4 mM magnesium sulfate, 2 mM EGTA and 20 mM Tris maleate buffer, pH 6.8) for 30 min.

The sarcomere lengths of these stretched fibers were kept unaltered by the friction force between the glass slide and the fibers, and a clamping effect of electrodes. The muscle fiber on the glass slide and covered with liquid paraffin oil was mounted on a sample holder, which was made of copper and was thermo-regulated with temperature-controlled circulating water (Komatsu/Yamato, Coolnics thermobath). The temperature near the muscle fiber was monitored with a thermister (NEC, B1 15).

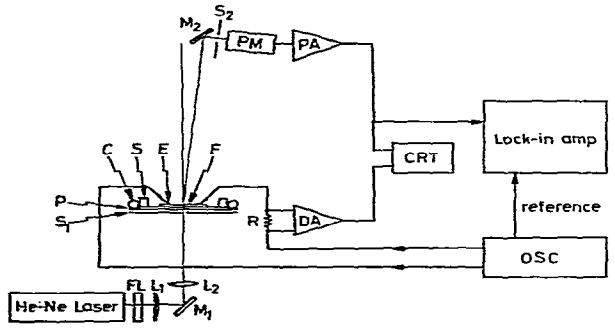

Fig. 1. Block diagram of experimental setup for the study under sinusoidal field. FL: red filter, L_1 and L_2: lenses, M_1 and M_2: mirrors, S_1 and S_2: slits, P: platform of an xy stage, S: sample holder made of copper block and filled with liquid paraffin oil, C: copper tubing for circulating thermoregulated water, E: electrodes, F: muscle fiber on a glass slide, PM: photomultiplier tube, PA: preamplifier, DA: differential amplifier, R: 1 kΩ resister, CRT: cathod ray tube, Lock-in Amp: lock-in amplifier with ω- and 2ω-modes, and OSC: RC-oscillator with a current booster.

2.3. Apparatus

2.3.1. Measurements of dispersion relations

The diffractometer we used was the same as the previous one [10]. The block diagram of the experimental setup is shown in fig. 1. A He-Ne gas laser (~7 mW) was used as a light source. Incident light was polarized parallel with the fiber axis. A red filter FL eliminated undesired light. A 632.8 nm laser beam was reflected by a surface mirror M_1, focussed by a lens L_2. The beam size at the fiber position P on an *xy* stage was 0.3 mm in diameter. A 0.5 mm slit S_1 eliminated undesired light. Diffraction lines were projected on a white screen (sample-to-screen distance; 114.6 mm) on which we could monitor the diffraction lines and determine the sarcomere length. The first order diffraction line was received by a photomultiplier tube (Hamamatsu TV., 1P28). The output current of the phototube was converted to voltage by a homemade pre-amplifier. A lock-in amplifier (Princeton Applied Research Corp., model 128) was used in its ω- or 2ω-mode to obtain the phase difference between the signal and the applied field to muscle fibers. The maximum band-width of the total system was 0.5 Hz—100 kHz. At the same time, the output of the phototube was monitored by an oscilloscope (Tektronix, model 5103N/D11). An RC oscillator (Kikusui Electronics Corp., model 417A) was used for a source of electric field. The output of a homemade current booster was fed to two thin platinum electrodes (coated with platinum black or not coated) *via* a 1 kΩ resistor as a current monitor. The booster had an offset control to minimize the dc component. The distance between the two electrodes was 2—5 mm. Since an electric field works as the driving (perturbing) force for the bending motion of thin filaments in a muscle fiber and the current produces a joule heat, the strength of the applied field should be as low as possible. Thus we made measurements at the condition of low electric field; the strength was typically 2 V_{pp}/cm and, at most, 10 V_{pp}/cm at higher frequency regions. Measurements of the dispersion relation were made at Nagoya University.

2.3.2. Measurements of decay rates

The apparatus we used was the same as the previous one [1], except that a signal processor having 400 bins (Sanei Instruments Co., Ltd., model 7S06A) was used in the present experiments. A light beam from a He-Ne laser (NEC, model 2026, 2 mW nominal) was focused by a lens on the fiber position. The beam size at the fiber position was about 0.3 mm in diameter. A 1 mm slit just before the fiber eliminated undesired light. Diffraction lines were projected on a white screen on which we could monitor the diffraction lines. The first order line was received by a photomultiplier tube (Hamamatsu TV., 1P28) and the output of the tube was fed to an oscilloscope (Nihonkoden, model VC7) and the signal processor *via* a homemade preamplifier. Two thin silver wires attached to the surface of the skinned fiber were connected to a stimulator (Nihonkoden, model MSE-3) *via* a 10 kΩ resistor as a current monitor. The stimulator was operated in its single or repeating mode. A train of pulses (interval, 0.5 s) from the stimulator triggered both the oscilloscope and the signal processor operated in its averaging mode, and the delayed output in a square form (duration, T = 50 ms—50 μs) was fed to the fiber. The rise and fall times of the square wave were shorter than 2 μs. The field strength was between 10 V/cm at longer durations and 100 V/cm at shorter durations. The

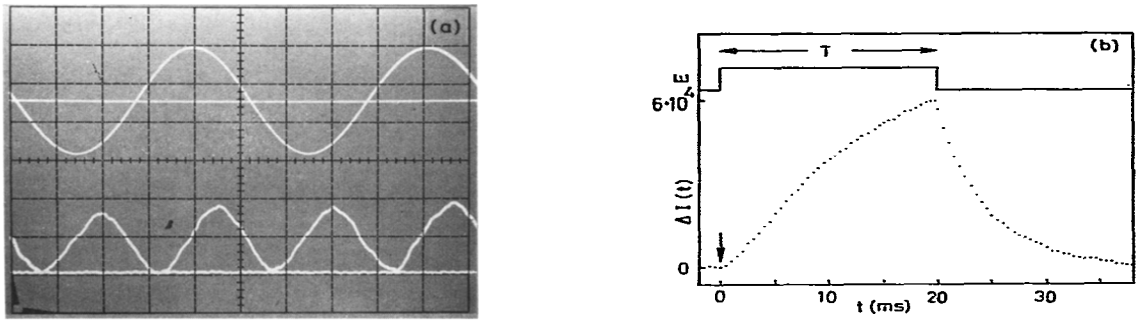

Fig. 2. Driving forces and responses. In (a) and (b), the upper trace shows the driving force and the lower trace the response. In (b), only 20% of the experimental data are shown.

temperature control was made by the same method as above. Measurements of the decay rates were made at the Jikei University School of Medicine.

3. Results

3.1. Driving force and response

To see the outline of our measurements, we show the wave forms of the driving force (or applied electric field) and the response. In fig. 2a, the upper trace shows the applied electric field and the horizontal line the zero level of the field. The lower trace shows the output of the phototube, of which frequency is twice that of the applied field, and the lowest line shows the output in the absence of applied field. The phase difference, $\phi_{2\omega}$, is given by the distance between the point of zero-crossing of applied field and the minimum point of the output wave. In fig. 2b, the upper trace shows the applied field in a square form, and the lower trace shows the output of the phototube. The decay rate can be obtained by cumulant expansion of the decay curve after turning off the field.

3.2. Elimination of very slow mode of motions

In the previous paper, we found that the decay curve of the excess intensity consists of, at least, two components; one is very slow ($\tau_s = 50$—100 ms) and the other is fast ($\tau_f = \tau_1/2 \simeq 5$ ms) [1]. The origin of this very slow component is not yet clear, but observations by a polarizing microscope suggested that the very slow mode came from the interfibril interaction. The squares in fig. 3 show the dispersion relation of a single fiber in paraffin oil at the sarcomere length of 6 μm, where thin and thick filaments have no overlap. This dispersion curve is far from the theoretical one and the "dispersion frequency" $\nu_1 \equiv \omega_1/2\pi$ which gives $\phi = \pi/4$ is very low. When we examined this fiber under the square field, the decay curve of the response contained the very slow component mentioned above. In fig. 3 are also shown the dispersion relations of the skinned fiber at the sarcomere length of 7.0 μm in liquid paraffin oil. The

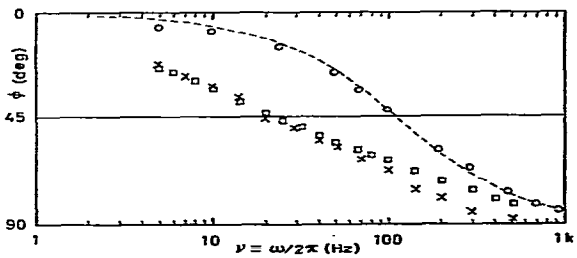

Fig. 3. The $\phi_{2\omega}$ versus ω relations of single and skinned fibers. (□): single fiber at the sarcomere length of 6 μm, (×): as-prepared skinned fiber at the sarcomere length of 7 μm, (○): the above fiber was treated with a saline solution (see 2.2) and swollen, and (- - -): the theoretical curve $\phi = \tan^{-1}(\omega\tau_1)$. 20°C.

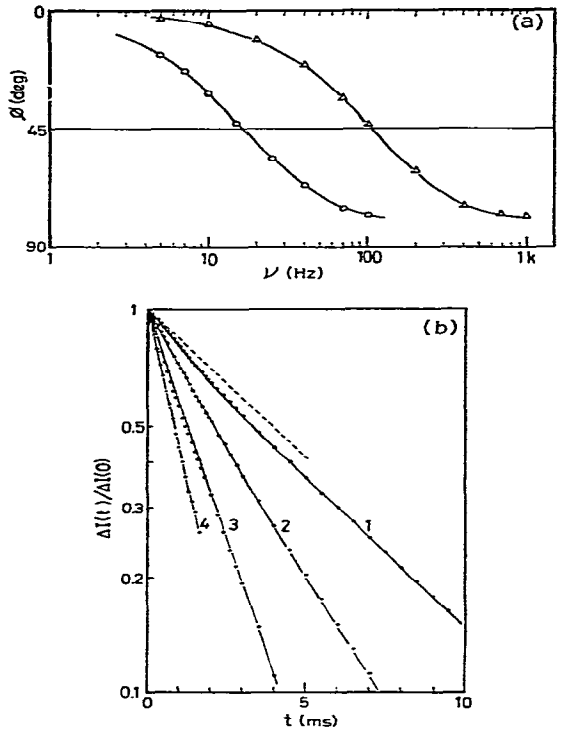

Fig. 4. Effect of Ca ions. (a) The ϕ_ω versus ω relations of; (o): skinned fiber at the sarcomere length of 7 μm was equilibrated with a saline solution containing 1 mM $CaCl_2$, and (Δ): the above fiber was treated with a saline solution containing 2 mM EGTA to remove free Ca ions from myofibrillar space. Field strengths at the measurements ≤ 1 V/cm, and 2 °C. (b) The decay curves of; 1: as-prepared skinned fiber of the sarcomere length of 8 μm, 2: a saline solution containing 10 mM EGTA (volume was several times that of the fiber) was poured to the above fiber, 10 square pulses of strength of 30 V/cm and duration of 10 ms were applied, the saline solution around the fiber was removed and the response was measured, 3: further treatment as above was made and measured, 4: further treatment was made, and - - - -: typical relaxation curve of swollen fibers. E = 30 V/cm, T = 10 ms and 20°C.

crosses are from an as-prepared skinned fiber, and the dispersion relation is very similar to that of the single fiber (squares in fig. 3). After saline solution was poured to the surface of the skinned fiber (see 2.2), the dispersion relation (circles in fig. 3) became very close to the theoretical one and the dispersion frequency shifted to about 100 Hz. Swelling of the fiber made the contribution from the very slow mode negligibly small. In fact, such a fiber gave a single exponential decay at, for example, T = 20 ms. In addition to the disappearance of the very slow mode, the response became very big. Probably, swelling made the space for motion of filaments wider. In the following experiments, we used swollen fibers.

3.3. Effect of applied field on sarcoplasmic reticulum

The dispersion frequency ν_1 of 100 Hz in fig. 3 gives $\tau_1 = 1/\omega_1 = 1.6$ ms, which is very small compared with those estimated previously [1] and given later, i.e., $\tau_1 \simeq 10$ ms measured under applied field in a square form. To see this discrepancy, the dispersion relation was measured with a skinned fiber which had been well equilibrated with a saline solution containin 1 mM $CaCl_2$. The result (circles in fig. 4a) gives a dispersion frequency ν_1 of about 16 Hz or τ_1 of 10 ms. This fiber was then treated with a 2 mM EGTA solution to remove free Ca^{2+} in the myofibrillar space, an the dispersion relation was again measured at very low field strength (≤ 1 V/cm). The result (triangles in fig. 4a) gives the dispersion frequency of 100 Hz or τ_1 of 1.6 ms. This change of ν_1 from 16 Hz to 100 Hz depending on the concentrations of Ca^{2+} was quite reversible. The results in fig. 4a clearly shows that the dispersion frequency strongly depends on the concentration of free Ca^{2+} in the myofibrillar space. The above result suggests that the τ_1 of about 10 ms in the previous study [1] corresponds to the relaxation time in the presence of free Ca^{2+}. Thus it is supposed that the strong field (10—100 V/cm in [1]) induced the release of Ca^{2+} from sarcoplasmic reticulum. Then a skinned fiber was washed with a saline solution containing 10 mM EGTA under the influence of applied square pulses of 30 V/cm in strength and 10 ms in duration. The relaxation time τ_1 for the treated fiber became shorter and shorter as the washing proceeded, and finally it was as short as 2 ms for applied field strength of 30 V/cm (fig. 4b). [Note that $\tau_1 = 2\tau_d$ where τ_d is the decay time.] The fiber was then equilibrated with a saline solution containing 1 mM $CaCl_2$. Then the fiber gave τ_1 of about 10 ms, which is the same as that of a swollen fiber without the above treatment.

In this way the apparent discrepancy was eliminate

it came from different concentrations of free Ca^{2+} in the myofibrillar space. Since the aim of the present study is to show the validity of our model discussed in [2], detailed study on the effect of Ca^{2+} will be described elsewhere. In the following, the measurements of the dispersion relations were made at very low field strength ($\lesssim 3$ V/cm), and those of the decay curves at relatively high strengths (10–50 V/cm). The latter is solely due to the limited ability of the signal processor used (see 3.5).

3.4. Electro-optical effect of ghost fibers

As we have discussed in [1], phoretic shifts of I-band positions by ξ from their lattice points may cause the intensity modulation of diffraction lines. The intensity changes due to this process can be written from eq. (22) in [1] as

$$\Delta I(u_n, t) \propto (-1)^n 2 f_I(u_n) f_A(u_n) [\cos(2\pi n \xi / L) - 1], \quad (3)$$

where the notation is the same as that in [2]. In [1], however, we excluded this possibility simply because intensities of all observable diffraction lines *increased* on application of the electric field, whereas the above $\Delta I(u_n, t)$ is positive or negative depending on the diffraction order index n. Now, if we use a ghost fiber where A-bands are absent, no or very small intensity change is expected to be observed provided that eq. (3) is valid.

At first, we measured the intensity increase $\Delta I_{\text{skinned}}$ of a well swollen skinned fiber at the sarcomere length of 6 μm for given strength and duration of applied field. Next, the same fiber was well treated with 1 M KCl and then the ionic strength was reduced to 0.1 M KCl. Initially, the fiber gave a relation $I_1 < I_2$ (fig. 5a) where I_n is the intensity of the nth order diffraction line. During the treatment with a high salt solution, the fiber gave a relation $I_1 \ll I_2$ (fig. 5b) and finally $I_1 \gtrsim I_2$ (fig. 5c). This process of the intensity change is considered to be the dissolving process of myosin from A-bands. After the treatment, optical anisotropy of the A-bands observed by a polarizing microscope was very much reduced. Although not complete, we could expect that A-bands were dissolved to a great extent after the treatment, i.e., $f_A(u) \simeq 0$. The treated fiber gave the intensity increase

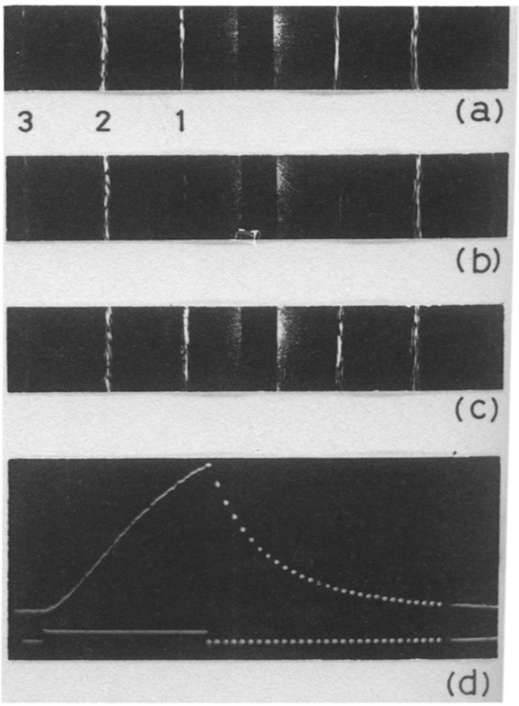

Fig. 5. (a) Optical diffraction pattern at the sarcomere length of 6 μm. Note that $I_1 \lesssim I_2$. (b) Diffraction pattern of the same fiber as in (a) but taken during the treatment with 1 M KCl. Note that $I_2 \gg I_1 \simeq 0$. (c) After the treatment (ghost fiber). Note that $I_1 \gtrsim I_2$. (d) Electro-optical response of a ghost fiber at $T = 10$ ms (see text).

ΔI_{ghost} very close to $\Delta I_{\text{skinned}}$ for the same strength and duration of the applied field; the results for five preparations were $\Delta I_{\text{ghost}} / \Delta I_{\text{skinned}} = 1.1, 1.0, 0.9, 1.3$ and 0.9. This experiment clearly shows that the intensity modulation is mainly due to some changes in I-bands and, at the same time, excludes the possibility of phoretic shifts of I-band positions. The following should be noted. Fig. 5d shows the intensity change of a treated fiber. The initial intensity increase is proportional not to time t but to t^2. This means that, even though $F^{(a)}(u_1)$ in eq. (25) of [2] is very large for the treated fiber, it holds that $\Delta I_1(u_1, t) < \Delta I_2(u_1, t)$ at longer durations T. But this is not necessarily so at higher frequencies or shorter durations, because ΔI_1 is proportional to, whereas ΔI_2 to the *square* of, $\cos(\varphi_k)$ or $[1 - \exp(-T/\tau_k)]$.

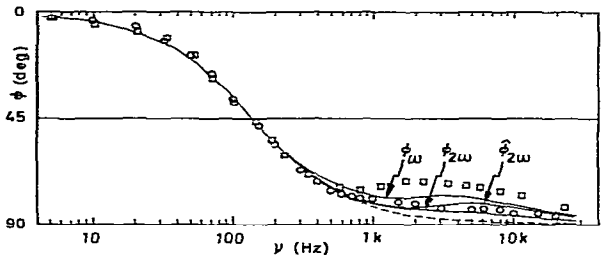

Fig. 6. The ϕ_ω versus ω and $\phi_{2\omega}$ versus ω relations of a swollen fiber at the sarcomere length of 7 μm. (□): ϕ_ω, (○): $\phi_{2\omega}$, (—): theoretical curves based on eqs. (63–65) in [2], and (- - -): the theoretical curve $\phi = \tan^{-1}(\omega\tau_1)$. 20°C.

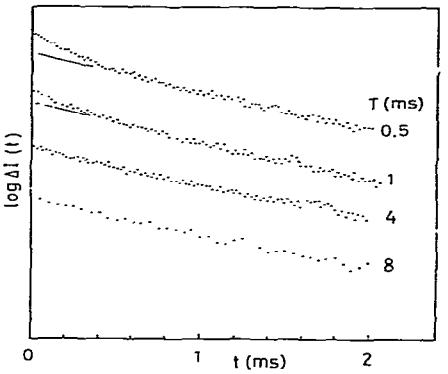

Fig. 7. Examples of decay curves at different durations of applied fields.

3.5. *On the second order mode of bending motions*

Fig. 6 shows the dispersion relations from 5 Hz to 30 kHz. At the main dispersion region ($\nu \leqslant 1$ kHz), both ϕ_ω and $\phi_{2\omega}$ coincide with the theoretical relation. At the higher frequency region ($\nu \geqslant 1$ kHz) where the contribution from the $k = 2$ mode is expected, experimental points largely deviate from the simple dispersion relation, $\phi = \tan^{-1}(\omega\tau_1)$. This deviation is strong evidence of the contribution from the $k = 2$ mode. Since the phase angle depended on the field strength and the absolute values of the deviation of experimental ϕ values at higher frequency region from theoretical ones depended on preparation of fibers, a quantitative comparison of experimental values with theoretical ones is difficult at present. However, the trend of the behaviors of the dispersion relations at the higher frequency region agrees with our predictions in [2]. Fig. 7 shows some examples of the decay curves at different durations T. It is clearly seen that at shorter T values the decay curves consist of two components; one is very fast and the other is fast (in the sense mentioned above). The shortest bin-width of our signal processor was only 20 μs. The contribution from the $k = 2$ mode with $1/\tau_2 = 5000\ s^{-1}$ would be included in the first 10–15 bins because the contribution decays to the 1/e of the initial value within 200 μs. Thus the cumulant expansion of the experimental data at shorter durations was made using, for example, first 50, 40, 30 and 20 points. Decreasing data points in the analysis gave increasing $(1/\tau)$ values as shown in fig. 8. The change of the small $(1/\tau)$ values at longer durations to the big ones at shorter durations came solely from the decreasing contribution of the $k = 1$ mode relative to the contribution of the $k = 2$ mode. Although the absolute values of the response at shorter durations or higher frequencies were very small, a fairly good agreement between experimental and theoretical results was obtained.

3.6. *Rise and decay curves of excess intensity*

We analyzed the rise curve $y(t)$ and the decay curve $\Delta i_D(t)$ by the procedure in 5.3 of [2]. To get $y(t)$ from the rise curve $\Delta i_R(t)$, the integration, eq. (55) in [2], was carried out after continuing the experimental

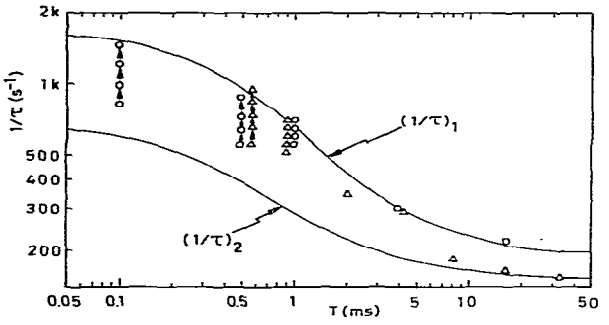

Fig. 8. The $(1/\tau)$ versus durations T obtained by the cumulant expansion method (for details, see text). Well swollen fibers at the sarcomere length of 7 μm, (—): theoretical curves based on eqs. (50,51) in [2], assuming $1/\tau_1 = 130$ and $1/\tau_2 = 5200\ s^{-1}$. 20°C.

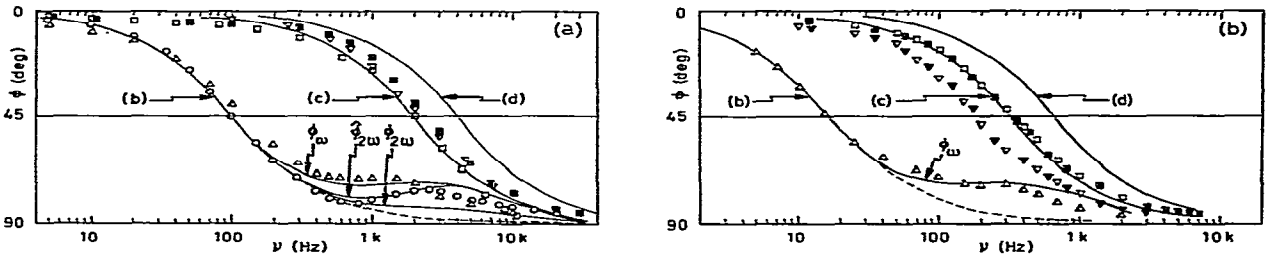

Fig. 9. The ϕ_ω versus ω and $\phi_{2\omega}$ versus ω relations of glycerinated muscle fibers at 20°C. (a) In the absence of free Ca^{2+}. (△): ϕ_ω and (○): $\phi_{2\omega}$ at the sarcomere length of 4.0 μm. (□,■): ϕ_ω in the absence of, and (▽): in the presence of, 4 mM pyrophosphate at the sarcomere length of 3.5 μm, (——): theoretical curves based on eqs. (63–65) and (- - -): $\phi = \tan^{-1}(\omega\tau_1)$. (b), (c) and (d) in the figure correspond to models b, c and d in [2] respectively. (b) In the presence of 0.1 mM free Ca^{2+}. (△): ϕ_ω at the sarcomere length of 4.0 μm. (□,■): ϕ_ω in the absence of, and (▽,▼): in the presence of, 4 mM pyrophosphate at the sarcomer length of 3.5 μm.

decay curve beyond the experimental range of time, assuming that the relaxation time was equal to that of the tail part of the experimental curve. The $(1/\tau)$ of $y(t)$ is 117 ± 1 and that of $\Delta i_D(t)$ is 108 ± 1 (s^{-1}) for the case of the response function shown in fig. 2b. Although the $(1/\tau)$ value of the former is larger than that of the latter by 8%, we conclude that the induced moment has no appreciable effect on the electro-optical effect.

3.7. Dispersion frequencies at different boundary conditions

To see the validity of our model from a different point of view, we show the results under different boundary conditions for the bending motion of thin filaments. When we use a *rigor* muscle fiber at the sarcomere length of, say, 3.5 μm, one end of each thin filament is not free but will be *hinged* or *fixed* at the overlap region. Then, the dispersion frequency of such fibers is expected to be twenty or more times higher than that of the fibers at sarcomere length of, say, 4 μm, where there is no overlap between thin and thick filaments (see fig. 7 in [2]). Since, at the sarcomere lengths shorter than 6 μm, the intensity of the first order line is very strong, so that we can measure the dispersion relations in the ω-mode of the lock-in detector. Fig. 9a shows the dispersion relations of glycerinated fibers at the sarcomere lengths of 3.5 μm (ω) and 4.0 μm (ω and 2ω) in the absence of free Ca^{2+}. In the case of squares in fig. 9a, the solution did not contain ATP, so that the fibers were not in the relaxed state. In the case of inverted triangles in fig. 9a, there existed 4 mM sodium pyrophosphate, so that the fiber was in the "relaxed" state. Fig. 9b shows the dispersion relations of glycerinated fibers at the sarcomere lengths of 4.0 μm (ω) and 3.5 μm (ω) in the presence of 0.1 mM free Ca^{2+}. In the case of squares in fig. 9b, the fiber was in the "rigor" state. In the case of inverted triangles in fig. 9b, on the other hand, there existed 4 mM pyrophosphate and 0.1 mM free Ca^{2+}, so that the fiber was in the "contracting" state. It is out of scope of the present study to discuss in detail the behaviors of the dispersion frequencies at different conditions; here we only emphasize that the gross features of the dispersion curves depending on the boundary conditions of the filament motion agree with the theoretical prediction in [2].

From eq. (60) in [2], we have, at the main dispersion region, $B_\omega \propto F^{(a)}(u_n)A'_1(u_n)$, where $A'_1(u_1)$ is positive at $L \geqslant 3.5$ μm, whereas $A'_1(u_2)$ is negative at $L < 6$ μm and positive at $L > 6$ μm. Since $F^{(a)}(u_1)$ is negative and $F^{(a)}(u_2)$ is positive at $L > 3$ μm, the phase (sign) of B_ω will be different by π for the first and the second order diffraction lines, provided that the sarcomere length is longer than 6 μm. The output of the lock-in detector in its ω-mode is proportional to $B_\omega \cos(\theta - \phi_\omega)$. We at first adjusted the phase shifter of the detector so as to give zero output, i.e., $\theta = \phi_\omega + \pi/2$, and then the phase shifter was switched to $\theta + \pi/2$ in order to know the phase of B_ω. In this way, we examined the phase of B_ω at $\nu = 100$ Hz and at the sarcomere lengths of 4.0 and 7.5 μm, and the above statement was confirmed.

4. Discussion

4.1. Validity of the model

Swelling of the fibers for elimination of the very slow mode of motions stated in 3.2 was not crucial because we could observe the dispersion relation very close to the theoretical one (i.e., $\phi = \tan^{-1}(\omega\tau_1)$) for intact fibers at very low field strengths. The only difficulty in the cases of intact fibers and of not swollen skinned fibers was the weakness of the desired response. In any case we have studied, strong field produced spurious effects on the dispersion relations.

Results on ghost fibers in 3.4 support our assumption that the electro-optical effect is due to some changes in I-bands. Our model discussed in [2] has taken account of no sophisticated problems such as interfilament, hydrodynamic and electrolytic interactions. Effects of such interactions are considered to be incorporated into an *effective* friction constant ζ and flexural rigidity ϵ. In this sense, our model for the electro-optical effect of muscle fibers is very crude. However, our model can explain well the experimental results presented here. As far as the main dispersion frequency region is concerned, the agreement between experimental and theoretical results is complete as seen in figs. 6 and 9. Results in 3.7 completely support our predictions (1), (2) and (4) discussed in [2]. The analysis in 3.6 showed that induced moments have no appreciable effect. This is relevant to the check point (5) discussed in [2]. As to the check point (3), i.e., as to the contribution from the $k = 2$ mode, the trend of the experimental results agrees with theoretical predictions in both ω- and 2ω-modes in figs. 6 and 9. Since the response became very weak at the higher frequency region, we applied a strong field. Discrepancies probably came from a growing contribution of $\hat{B}_{2\omega}$ in eq. (58) of [2] and partly from joule heating. Of course, the crudeness of the model may partly be responsible for the descrepancies.

Experimental results in fig. 8 suggest that at longer durations T (and hence lower field strengths) the main contribution to the response came from $\Delta I_2(u_1, t)$, whereas at shorter durations T (and hence higher field strengths) the main contribution came from $\Delta I_1(u_1, t)$ probably due to the enhancement of ΔI_1 through a parameter η in eq. (47) of [2]. Actually we can see in fig. 4 of [1] that the initial increase of the excess intensity is proportional to time t at higher field strengths and to t^2 at lower field strengths. Anyway, the fact that the experimental results lie between theoretical curves of $(1/\tau)_1$ and $(1/\tau)_2$ supports our model. We believe that our basic assumption of a semiflexible thin filament model is valid.

4.2. On experimental techniques

We have studied the electro-optical effect of muscle fibers by two methods, i.e., applied field in sinusoidal and square forms. Theoretically, both methods should give the same information. In practice, however, each method has its own merits and demerits. Merits of one method are the demerits of the other, and the two methods are complementary.

In the case of the sinusoidal field, merits of the method are: (1) we can measure the phase retardation, and not the intensity itself, of the response, which is free from accidental intensity changes during measurements, and (2) we can measure the dispersion relations of ω- and 2ω-modes separately if we use a lock-in detector, which is free from restriction on setting of sarcomere lengths.

In the case of square field, merits of the method are: (1) this method is very sensitive to the contribution of the $k = 2$ mode as shown in fig. 8, (2) we can easily follow the rising characteristics of the response, and (3) the problem of joule heating can easily be avoided if we apply an electric field in a suitable interval.

4.3. Flexural rigidity of thin filaments in vivo

Since we made no detailed study of the effect of field strengths on the relaxation time in the case of a square field, the following discussion is concerned with the case of a sinusoidal field. As shown by the dashed lines in figs. 6 and 9, the contribution from the $k = 2$ mode is negligibly small at the frequency $\nu_1 \equiv \omega_1/2\pi$ where $\phi_{2\omega}$ (or ϕ_ω) $= \pi/4$ (the dispersion frequency of the $k = 1$ mode). Then we have [1,2]

$$\omega_1 = 1/\tau_1 = \lambda_1/\zeta = \epsilon(0.6\,\pi/a)^4/\zeta, \tag{4}$$

or

$$\epsilon = [\zeta a^4/(0.6\,\pi)^4]\omega_1 = [k_B T a^3/D(0.6\,\pi)^4]\omega_1, \tag{5}$$

where the Stokes–Einstein relation, $D = k_B T/\zeta a$, was assumed. Then we have the flexural rigidity ϵ for the length of a thin filament of $a = 1$ μm (for frog) and $D = 1.0 \times 10^{-8}$ cm^2/s (at 20°C)

$$\epsilon = 3.1 \times 10^{-19} (\eta_T/\eta_{293}) \omega_1, \quad (6)$$

where ω_1 is in rad/s unit and η_T is the viscosity of *water* at T K. The ϵ values at 20°C are 3.1×10^{-17} dyn·cm^2 in the presence of, and 1.9×10^{-16} dyn cm^2 in the absence of, Ca^{2+} in the myofibrillar space. As to the temperature dependence of ϵ values, the activation enthalpies were measured [manuscript in preparation]. They were about 5 kcal/mole in the presence of, and about 10 kcal/mole in the absence of, Ca^{2+}. We must note here that the ϵ values estimated above do not necessarily correspond to those of a *single* thin filament, but rather to apparent ones in the dense packing of thin filaments. However, the present ϵ values are believed to be good estimates of the flexural rigidity of a thin filament both *in vivo* and *in vitro*.

The present ϵ value in the presence of Ca^{2+} is very close to those of previous results [1,3,5,6,12], but that in the absence of Ca^{2+} is much bigger than the previous one [6]. The activation enthalpy of about 5 kcal/mole in the presence of Ca^{2+} is also very close to the previous ones [11,12], whereas that of about 10 kcal/mole in the absence of Ca^{2+} is very big. The previous measurements are concerned with F-actin *in vitro*, so that the effect of a tropomyosin/troponin system on thin filaments must be taken into account for the comparison of the ϵ values. This point will be discussed in 4.4.

4.4. Concluding remarks

Thin filaments consist of F-actin, tropomyosin and troponin. Tropomyosin molecules are believed to associate with F-actin in such a manner that they settle down in the grooves of F-actin helix [13]. Consequently the temperature dependence of the flexural rigidity of thin filaments should originate at least from (1) loosening of actin-actin bonds, (2) loosening of actin-tropomyosin bonds and (3) the increase of the flexibility of tropomyosin rods. Loosening of actin-actin bonds will be responsible for the increase of the flexibility of F-actin alone with rising temperature [11,12]. Loosening of actin-tropomyosin bonds is expected from the experimental fact that rabbit tropomyosin dissociates from rabbit F-actin *in vitro* above 37°C [14]. Even below the dissociation temperature, bond loosening should occur. The increase of the flexibility of tropomyosin rods with rising temperature is also expected from the decrease of the helix contents of tropomyosin rod [14]. Thus, the observed change of the flexibility of thin filaments is a result of composite contributions from various origins.

It is interesting to note here the following. In extremely stretched fibers of a frog, $I_1 < I_2$ was observed as mentioned before. When the temperature of the fiber was raised, $I_1 \geqslant I_2$ was observed above 30°C. When we examined extremely stretched fibers of a rabbit or a guinea pig, such a big change in intensities was not observed even at 35°C.

The present method seems to be very powerful for studying the dynamics of thin filaments *in vivo*. We will discuss elsewhere the physiological implications of the flexibility of thin filaments after we apply this method to muscle fibers from both poikilo- and homoi-thermic animals under various environmental conditions.

References

[1] Y. Umazume and S. Fujime, Biophys. J. 15 (1975) 163.
[2] S. Fujime and S. Yoshino, Biophys. Chem. 8 (1978) 305.
[3] S. Fujime, J. Phys. Soc. Japan 29 (1970) 751.
[4] S. Fujime and M. Maruyama, Macromolecules 6 (1973) 237.
[5] S. Fujime and S. Ishiwata, J. Mol. Biol. 62 (1971) 251.
[6] S. Ishiwata and S. Fujime, J. Mol. Biol. 68 (1972) 511.
[7] C.T. O'Konski and A.J. Haltner, J. Amer. Chem. Soc. 78 (1956) 3604.
[8] D.E. Koppel, J. Chem. Phys. 57 (1972) 4814.
[9] R. Natori, Jikeikai Med. J. 1 (1954) 18.
[10] S. Fujime, Biochim. Biophys. Acta 379 (1975) 227.
[11] S. Ishiwata, PhD thesis (Nagoya University) (1975).
[12] T. Takebayashi, Y. Morita and F. Oosawa, Biochim. Biophys. Acta 492 (1977) 357.
[13] S. Ebashi and M. Endo, in: Progress in Biophysics and Molecular Biology, vol. 18 (1968) p. 123.
[14] H. Tanaka and F. Oosawa, Biochim. Biophys. Acta 253 (1971) 274.